On Hydromagnetic Boundary Layer of Casson Fluid Over Porous Inclined Magnetized Surface With Radiation and Convective Boundary Conditions

Golbert Aloliga*[1] [iD], Ibrahim Yakubu Seini[2] [iD] and Rabiu Musah[2] [iD]

[1] *CK Tedam University of Technology and Applied Sciences, 00233, Navrongo, Upper East Region, Ghana*
[2] *School of Engineering, University for Development Studies, Tamale, Nyankpala Campus, 00233, Northern Region, Ghana*
*Corresponding author: aloligagolbert@gmail.com

Abstract. The boundary layer of a non-Newtonian Casson fluid flow over inclined porous magnetized surfaces with radiation and convective boundary conditions have been considered. The effects of the magnetic field, thermal radiation, convection with temperature fields at the boundaries of the surface are considered. The governing models have been transformed to ordinary differential equations employing the similarity approach. The effects of surface magnetization along with bulk parameters on the flow are presented in tables. The thickness of the thermal boundary layer has been enhanced due to the induced magnetic field leading to considerable improvement in the rate of heat transfer. The induced magnetized surface showed a similar influence on the skin friction, Nusselt number, and the Sherwood number. The study, therefore, recommends the incorporation of magnetized surfaces in MHD flows for efficient flows control.

Keywords. Magnetized plate, Non-Newtonian Casson fluid, Convective boundary conditions, Internal heat generation

Mathematics Subject Classification (2020). 76-10, 76A05, 76D05

1. Introduction

Due to the numerous engineering applications of non-Newtonian Casson fluids, researchers have invested a lot of time in studying the flow of the fluid. The applications include, food processing, photodynamic therapy, nuclear cooling, as well as in biological systems. Casson fluids are a type of non-Newtonian fluids with examples as; jelly, tomato sauce, human blood, honey, etc. The nonlinear constitutive relation of Casson fluids has been found appropriate to explain the flow curvatures of suspended pigments within the lithographic which is used for the preparation of inks and silicon suspension [5, 17]. The shear strain-shear rate relation given by Casson adequately portrays the properties of numerous polymers over a wide range of shear rates [16]. Many computational methods have been used to study and analyze various flow phenomena involving steady and unsteady flows. The Homotopy analysis method (HAM) [13] has been used to investigate the unsteady flow and heat transfer of Casson fluid over a flat plate moving with the parallel free stream using. The standard Newton-Raphson shooting method alongside the fourth-order Runge-Kutta integration algorithm has been explored by [2]. The mixed convection stagnation-point flow of a non-Newtonian Casson fluid over a stretching sheet with convective boundary conditions has been investigated by Hayat *et al.* [7] whilst Bhattacharyya [4] examined boundary layer flow of Casson fluid over a stretching/shrinking sheet and observed that, the value of the finishing product depended on the rate of temperature transmit from the stretching plane. The Laplace transform method has been used to investigate heat transfer phenomena on time subservient Casson fluid, [9]. The characteristics of the same fluid on a stretching cylinder with the appearance of nanoparticles [12] have been reported. The impressions of heat source/sink with the chemical reaction for non-Newtonian Casson fluid [8] and the influence of hydromagnetic free convection with radiation [11] on viscous dissipative Casson fluid in a non-Darcian porous medium have significant applications in industry. Other researchers have made significant contributions [1, 10, 15] by examining the impact of diversified physical parameters on hydromagnetic Casson fluid flow by considering various boundary criteria.

This article focuses on the hydromagnetic boundary layer flow of Casson fluid over a porous inclined magnetized surface with radiation and convective boundary conditions as it is frequently encountered in most cooling and manufacturing processes. The rest of the article will be organized as follows: Section 2 presents the Mathematical Modeling process with its appropriate assumptions followed by Similarity Analysis in Section 3. The Numerical Procedure and Results Analysis are presented in Sections 4 and 5, respectively while Conclusions and Recommendations are outlined in Sections 6 and 7, respectively.

Nomenclature

u, v, w	Velocity components along x, y and z axes (m/s)
B_0	Applied magnetic field (Wb/m^2)
t	Time (s)
T_w	Wall temperature (K)
U_0	Characteristic velocity (m/s)

C	Concentration (kg/m^3)
g	Acceleration due to gravity (m/s^2)
T	Temperature of the Casson fluid (K)
$f(\eta)$	Similarity function
$\theta(\eta)$	Dimensionless temperature
q_r	Radiation flux distribution in fluid (W/m^2)
Nu	Nusselt number
Sh	Sherwood number
k	Thermal conductivity of the fluid (W/m/K)
Pr	Prandtl number
q'	Volumetric heat generation (w)
M_s	The magnetic parameter at the surface
M_b	The magnetic parameter at the bulk
Br	The Brinkmann parameter

Greek Symbols

β	Casson parameter
ρ	Fluid density
η	Dimensionless similarity variable
λ	Internal heat generation parameter
σ	Electrical conductivity of the base fluid (m^2/s)
α	Thermal diffusivity
ω	Casson order
v	Kinematic viscosity (m^2/s)
ψ	Stream function (m^2/s)
μ	Fluid viscosity (kg/m/s)
β_T	The thermal coefficients (1/K)
β_C	Concentration expansion coefficients (1/kg m^3)

2. Mathematical Model

From Figure 1, we considered a steady electrically conducting Casson fluid flow over an inclined permeable stretched surface at $y = 0$, in the existence of a slanting magnetic field. The x-axis is taken along the bearing of the sheet and the y-axis perpendicular to it. Assuming the fluid occupies the half space $y > 0$ and the mass transfer phenomenon with chemical effect. The flow is subjected to a constant applied magnetic field B_0 in the y-direction. The magnetic Reynolds number is considered to be very small so the induced magnetic field is negligible in comparison to the applied magnetic field. The divergent velocity u_w, from the stretching surface, is assumed to differ proportionally to the distance x so that, $u_w = ax^m$, where a and m are constants.
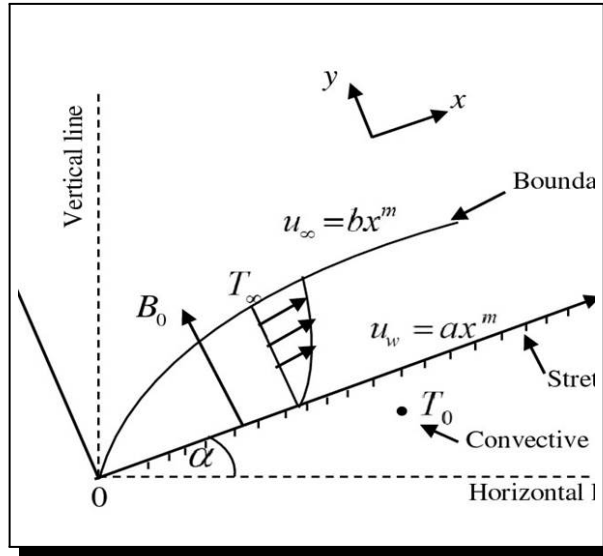
Figure 1. Schematic diagram of the problem

The rheological equation of state for anisotropic flow [6] of a Casson fluid can be expressed as:

$$\begin{cases} 2\left(\mu_B + \frac{P_y}{\sqrt{2\pi}}\right)e_{ij}, & \mu > \pi_c, \\ 2\left(\mu_B + \frac{P_y}{\sqrt{2\pi}}\right)e_{ij}, & \mu < \pi_c. \end{cases} \tag{1}$$

In eq. (1), π is the product of the component of deformation rate with itself, where $\pi = e_{ij}e_{ij}$ and e_{ij} is the (i,j)th component of the deformation rate, π_c is the critical value of this product based on the non-Newtonian model, μ_B is the plastic dynamic viscosity of the non-Newtonian fluid and P_y is the yield stress of the fluid.

Supposing that, the velocities along the x and y axes are respectively represented by u and v, with T being the temperature and C, the concentration of the fluid, then the governing models of the steady Casson fluid is obtained as:

$$\frac{\partial u}{\partial x} + \frac{\partial v}{\partial y} = 0, \tag{2}$$

$$u\frac{\partial u}{\partial x} + v\frac{\partial u}{\partial y} = \mathcal{V}\left(1 + \frac{1}{\beta}\right)^{\omega}\frac{\partial^2 u}{\partial y^2} + g\beta_t(T - T_\infty)\cos(\alpha) + g\beta_t(C - C_\infty)\cos(\alpha) + \frac{\sigma B_0^2}{\rho}u, \tag{3}$$

$$u\frac{\partial T}{\partial x} + v\frac{\partial T}{\partial y} = \alpha\frac{\partial^2 T}{\partial y^2} + \frac{\mathcal{V}}{c_p}\left(1 + \frac{1}{\beta}\right)^{\omega}\left(\frac{\partial u}{\partial y}\right)^2 - \frac{\alpha}{k}\frac{\partial q_r}{\partial y} + \frac{\lambda_T}{\rho c}(T - T_\infty) + \frac{\sigma B^2}{\rho}u^2, \tag{4}$$

$$u\frac{\partial C}{\partial x} + v\frac{\partial C}{\partial y} = D\left(\frac{\partial^2 C}{\partial y^2}\right) - \lambda_2(C - C_\infty), \tag{5}$$

with boundary conditions:

$$\left.\begin{aligned} &u = u_w = U_0(B)ax^m, \;\; V = V_w, \;\; T = T_W, \;\; C = C_W \text{ as } y = 0, \\ &u \to 0, \;\; T \to T_\infty, \;\; C \to C_\infty \text{ as } y \to \infty \end{aligned}\right\} \tag{6}$$

3. Similarity Analysis

Introducing the stream function defined as $\psi = x^m\sqrt{av}f(\eta)$ and a dimensionless variable, $\eta = y\sqrt{\frac{a}{v}}$, and noting that the velocity components relate to the stream function in the usual way as

$$u = \left(\frac{\partial\psi}{\partial y}\right)_x \quad\text{and}\quad v = \left(\frac{\partial\psi}{\partial x}\right)_y. \tag{7}$$

Eq. (7) simplifies to:

$$u = ax^m f' \quad\text{and}\quad v = -m\sqrt{avx^{m-1}}f. \tag{8}$$

Eq. (2) is satisfied identically by eq. (8).

Introducing the similarity variables, $T = T_o\theta + T_\infty$, and $C = (C_w - C_\infty)\phi + C_\infty$, eqs. (3), (4), and (5) transform into:

$$\left(1+\frac{1}{\beta}\right)^\omega f''' - mf'^2 + mff'' + \mathrm{Gr}\,\theta\cos(\alpha) + \mathrm{Gm}\,\theta\cos(\alpha) + M_b f' = 0, \tag{9}$$

$$\left(1-\frac{4}{3}\mathrm{Ra}\right)\theta'' + m\mathrm{Pr}\,f\theta' + \mathrm{Br}\left(1+\frac{1}{\beta}\right)^\omega f''^2 + Q\theta + \mathrm{Pr}\,M_b f'^2 = 0, \tag{10}$$

$$\frac{1}{\mathrm{Sc}}\phi'' + mf\phi' + \lambda\phi = 0, \tag{11}$$

where the number of times a function is differentiated with respect to η is represented by the prime symbol(s). The local Grashof and the modified Grashof numbers are respectively represented by $\mathrm{Gr} = \frac{g\beta_t T_0}{a^2 x^{2m-1}}$ and $\mathrm{Gm} = \frac{g\beta_C C_0}{a^2 x^{2m-1}}$, $\lambda = \frac{\gamma}{ax^{m-1}}$ is the reaction rate parameter, $\mathrm{Pr} = \frac{v}{\alpha}$ represents the Prandtl number, $\mathrm{Ra} = \frac{4\sigma^* t_\infty^3}{\kappa K'}$ represents the thermal radiation parameter, $\mathrm{Br} = \mathrm{Pr}\,\mathrm{Ec}$.

$\mathrm{Ec} = \frac{a^2 x^m}{c_p}$ is the Eckert number, $Q = \frac{\lambda_T}{\rho c a x^{m-1}}$ is heat source dimensionless parameter, $M_b = \frac{\sigma B^2 a x^{m+1}}{T_0\rho}$ is the magnetization at the plate and $\mathrm{Sc} = \frac{v}{D}$ is the Schmidt number.

The convective boundary conditions are transformed as follows:

When $y = 0$, $\eta = 0$, $u = u_w$, $v = V_w$, $C = C_w$ and $T = T_w$.

Thus, $f'(0) = 1 - M_s$, $f(0) = f_w$, $\theta(0) = 1$, $\phi(0) = 1$ as $\eta = 0$.

As $y \to \infty$, $\eta \to \infty$, $f'(\infty) = 0$, $\theta(\infty) = 0$, $\phi(\infty) = 0$, \tag{12}

where $M_s = \frac{\sigma\bar{B}_0^2}{a\rho/L}$ is the magnetic field at the surface of the plate.

4. Numerical Procedure

Equations (9), (10), and (11) are the coupled ordinary differential equations whilst eq. (12) is the corresponding boundary conditions. These coupled ODEs are observed to be of third higher-order and therefore difficult to solve directly. To obtain a simplified solution, we employ the order of reduction techniques by letting:

$$\left.\begin{aligned}&f = x_1, \ f' = x_2, \ f'' = x_3, \ f''' = x_4, \ \theta = x_5, \ \theta' = x_6,\\&\phi = x_7, \ \phi' = x_8\end{aligned}\right\} \tag{13}$$

Eqs (9), (10), and (11) are then reduced to first-order ODEs as

$$x_1' = x_2, \tag{14}$$

$$x_2' = x_3, \tag{15}$$

$$x_3' = \frac{1}{\left(1 + \frac{1}{\beta}\right)^\omega}(mx_2^2 - m(xx_3) - \mathrm{Gr}\,x_5 - \mathrm{Gm}\,x_7 - M_b x_2), \tag{16}$$

$$x_5' = \frac{1}{\left(1 + \frac{4}{3}\mathrm{Ra}\right)}\left(-m\,\mathrm{Pr}(x_1 x_6) - \mathrm{Br}\left(1 + \frac{1}{\beta}\right)^\omega x_3^2 - Q x_5 - \mathrm{Pr}\,M_b x_2^2\right), \tag{17}$$

$$x_7' = -\mathrm{Sc}(mx_1 x_8 + \lambda x_7). \tag{18}$$

The boundary conditions in eq. (12) become:

$$\left.\begin{array}{l} x_2(0) = 1 - M_s, \quad x_1(0) = 0, \quad x_5(0) = 1, \quad x_7(0) = 1, \quad \text{as } \eta = 0, \\[2mm] x_2(\infty) = 0, \quad x_5(\infty) = 0, \quad x_7(\infty) = 0, \quad \text{as } \eta \longrightarrow \infty \end{array}\right\} \tag{19}$$

With the aid of the MAPLE-19 software package, numerical and graphical codes were developed and implemented. A step size of $\Delta h = 0.001$ for a convergence criterion of 10^{-6} for all the cases was assumed. The highest value of η_∞ to each parameter was known when the values of the unidentified boundary conditions remain unchanged to a final loop with an error, not more than 10^{-6}.

5. Result Analysis

5.1 Numerical Results

To ensure the correctness of the applied numerical scheme, we contrast our derived results corresponding to the skin-friction coefficient ($f''(0)$) and the local Nusselt number ($-\theta'(0)$) for steady Casson fluid flow with thermal radiation effect with the results of Arthur *et al.* [3], and Salahuddin *et al.* [14] in Table 1. The presentation indicates a perfect agreement to five decimal places.

Table 1. Comparison of values of $-\theta'(0)$ for different values of Pr

Pr	Arthur *et al.* [3]	Salahuddin *et al.* [14]	Present study $M_s = 0$, $M_b > 0$	Present study M_s, $M_b > 0$
1.5	0.591382	0.591382	0.591383	0.492951
1.7	0.668983	0.668983	0.668984	0.569908
1.9	1.176499	1.176499	1.176500	1.065134
2.0	3.231228	3.231228	3.231228	2.833451

5.1.1 Skin Friction and Rate of Heat and Mass Transfer without Surface Magnetization ($M_{S=0}$)

The results of varying parameters on the local skin friction coefficient, the local Nusselt number, and the local Sherwood number when the surface magnetization is zero are presented in Table 2 and 3. It is worth noting that enhancing M_b, Gm, λ and Br values appreciates the skin friction and decreases with increasing values of Pr, Ra, Sc, β, and fw. This means that the combined effect of high viscosity over magnetic force induced Lorenz force, and suction at the surface of the sheet causes the local skin friction to increase and the combined effect of high thermal diffusion over mass diffusion, buoyancy forces, the Casson parameter of the fluid causes the local skin friction at the surface of the plate to surge up. Similarly, increasing values of Pr, λ, Gm, Br, ω, M_b, and Ra enhance the rate of heat transfer at the surface and reduces with increasing values of β, n, α, Gm, Sc, and fw. Moreover, it is observed that the rate of mass transfer increases with increasing values of Pr, λ, M_b, Sc, and Ra; and decreases with increasing values of Sc, Br, Gm, β, and Gr.

Table 2. Skin friction coefficient $[f''(0)]$, Nusselt $[-\theta'(0)]$ and Sherwood $[-\phi'(0)]$ numbers for $m = \text{Gr} = \text{Gm} = \omega = 1.0$, $Q = 0.1$

Pr	λ	Br	α	Ra	M_b	β	Sc	fw	$f''(0)$	$-\theta'(0)$	$-\phi'(0)$
0.90	1.0	0.1	30	0.1	1.0	0.7	0.8	0.1	-0.106886	-0.373511	-0.238799
0.91	1.0	0.1	30	0.1	1.0	0.7	0.8	0.1	-0.106944	-0.378487	-0.239034
0.95	1.0	0.1	30	0.1	1.0	0.7	0.8	0.1	-0.107160	-0.398408	-0.239923
0.90	1.1	0.1	30	0.1	1.0	0.7	0.8	0.1	-0.097395	-0.381779	-0.495663
0.90	1.2	0.1	30	0.1	1.0	0.7	0.8	0.1	-0.082521	-0.395096	-0.881424
0.90	1.0	0.2	30	0.1	1.0	0.7	0.8	0.1	-0.105827	-0.398629	-0.236659
0.90	1.0	0.6	30	0.1	1.0	0.7	0.8	0.1	-0.103705	-0.448668	-0.232410
0.90	1.0	0.1	32	0.1	1.0	0.7	0.8	0.1	0.397990	-0.654976	0.069228
0.90	1.0	0.1	33	0.1	1.0	0.7	0.8	0.1	-0.252225	-0.297674	-0.455439
0.90	1.0	0.1	30	0.2	1.0	0.7	0.8	0.1	-0.107498	-0.459469	-0.241753
0.90	1.0	0.1	30	0.3	1.0	0.7	0.8	0.1	-0.108016	-0.583061	-0.244710
0.90	1.0	0.1	30	0.1	2.0	0.7	0.8	0.1	-0.616050	0.486578	0.412772
0.90	1.0	0.1	30	0.1	3.0	0.7	0.8	0.1	-0.918361	0.882319	0.769433
0.90	1.0	0.1	30	0.1	1.0	0.8	0.8	0.1	-0.106975	-0.355842	-0.265032
0.90	1.0	0.1	30	0.1	1.0	0.9	0.8	0.1	-0.106745	-0.341511	-0.290292
0.90	1.0	0.1	30	0.1	1.0	0.7	0.9	0.1	-0.111707	-0.368068	-0.203034
0.90	1.0	0.1	30	0.1	1.0	0.7	1.0	0.1	-0.115426	-0.364218	-0.174236
0.90	1.0	0.1	30	0.1	1.0	0.7	0.8	0.2	-0.132162	-0.288701	-0.142648

Table 3. Skin friction coefficient $[f''(0)]$, Nusselt $[-\theta'(0)]$ and Sherwood $[-\phi'(0)]$ numbers for $\text{Pr} = 0.9$, $m = \lambda = 1.0$, Br $= 0.1$, $\alpha = 30°$, Ra $= 0.1$, $M_b = 1$, $\beta = 0.7$, Sc $= 0.8$, fw $= 0.1$

Gr	Gm	M_s	ω	Q	$f''(0)$	$-\theta'(0)$	$-\phi'(0)$
1.0	1.0	1.0	1.0	0.1	-0.158454	-0.199260	-0.047310
2.0	1.0	1.0	1.0	0.1	-0.043016	-0.407875	-0.176285
3.0	1.0	1.0	1.0	0.1	0.021767	-0.444080	-0.122790
1.0	2.0	1.0	1.0	0.1	-0.047351	-0.404040	-0.182269
1.0	3.0	1.0	1.0	0.1	0.008218	-0.432164	-0.138721
1.0	1.0	3.0	1.0	0.1	1.428115	-8.184817	0.428475
1.0	1.0	4.0	1.0	0.1	1.963552	-11.582677	0.486297
1.0	1.0	1.0	2.0	0.1	-0.098321	-0.585596	-0.090893
1.0	1.0	1.0	3.2	0.1	-0.094497	-0.790231	-0.044984
1.0	1.0	1.0	1.0	0.2	-0.103600	-0.510793	-0.233892
1.0	1.0	1.0	1.0	0.3	-0.099806	-0.664886	-0.228300

5.1.2 Skin Friction and Heat and Mass Transfer Rates With Surface Magnetization

The results of varying parameter values with the surface magnetization and bulk magnetization of the fluid on the local skin friction coefficient, the local Nusselt number, and the local Sherwood number, are shown in Table 4 and 5. It is observed that the skin friction increases with increasing values of M_b, M_s, λ Gm, Gr, Br, β, Sc and fw; and decreases with increasing values of Pr, Ra, and n. This means that the combined effect of high viscosity over magnetic force, the induced Lorenz force, and suction at the surface of the sheet increases the local skin friction; and the combined effect of high thermal diffusion over mass diffusion, buoyancy forces, chemical species of the fluid decreases the local skin friction at the surface of the plate. Similarly, the rate of

heat transfer at the plate surface increases with an increase in parameter values of Pr, λ, Ra, Br, Gm, Gr, M_b and reduces with increasing values of β, n, Sc, and Gm. Moreover, it is observed that the rate of mass transfer increases with increasing values of Pr, λ, M_s, and Ra; and decreases with increasing values of Br, n, Sc, Gr, Gm, λ, and β.

Table 4. Skin friction coefficient [$f''(0)$], Nusselt [$-\theta'(0)$] and Sherwood numbers [$-\phi'(0)$] for various values of parameters for Gr = 1.0, Gm = 1.0, Mb = 0.1, Ms = 0.5, fw = 0.1, Q = 0.1, ω = 1

Pr	λ	Br	α	Ra	m	β	Sc	$f''(0)$	$-\theta'(0)$	$-\phi'(0)$
0.90	1.0	0.1	30	0.1	1	0.7	0.8	0.199490	0.529559	−5.617663
0.95	1.0	0.1	30	0.1	1	0.7	0.8	0.199332	0.545584	−5.628636
0.98	1.0	0.1	30	0.1	1	0.7	0.8	0.199234	0.554991	−5.634695
0.90	1.2	0.1	30	0.1	1	0.7	0.8	0.349885	0.537833	−9.809549
0.90	1.4	0.1	30	0.1	1	0.7	0.8	0.383022	0.537091	−11.968804
0.90	1.0	0.2	30	0.1	1	0.7	0.8	0.199438	0.514436	−5.602335
0.90	1.0	0.3	30	0.1	1	0.7	0.8	0.199387	0.499323	−5.587012
0.90	1.0	0.1	32	0.1	1	0.7	0.8	0.462133	.612251	−0.612251
0.90	1.0	0.1	35	0.1	1	0.7	0.8	−0.434813	0.435889	0.957072
0.90	1.0	0.1	30	0.2	1	0.7	0.8	0.198947	0.577848	−5.647478
0.90	1.0	0.1	30	0.3	1	0.7	0.8	0.198129	0.641518	−5.677694
0.90	1.0	0.1	30	0.1	3	0.7	0.8	−0.327415	0.982353	−0.032824
0.90	1.0	0.1	30	0.1	4	0.7	0.8	−0.421524	1.177021	0.420671
0.90	1.0	0.1	30	0.1	1	0.8	0.8	0.211357	0.531754	−5.6070781
0.90	1.0	0.1	30	0.1	1	1.0	0.8	0.221705	0.533615	−5.6008327
0.90	1.0	0.1	30	0.1	1	0.7	0.9	−0.424526	1.174947	0.5089761
0.90	1.0	0.1	30	0.1	1	0.7	1.0	−0.426891	1.173364	0.590348

Table 5. Skin friction coefficient [$f''(0)$], Nusselt [$-\theta'(0)$] and Sherwood numbers [$-\phi'(0)$] for values of parameters for Pr = 0.9, Pr = 1.0, Br = 0.1, λ = 30, Ra = 0.1, m = 1, β = 0.7, Sc = 0.8

Gr	Gm	M_b	M_s	fw	Q	ω	$f''(0)$	$-\theta'(0)$	$-\phi'(0)$
1.1	1.0	0.1	0.5	0.1	0.1	1	0.202467	0.529721	−5.591746
1.2	1.0	0.1	0.5	0.1	0.1	1	0.205445	0.529881	−5.565884
1.0	1.1	0.1	0.5	0.1	0.1	1	0.205087	0.529974	−5.125902
1.0	1.2	0.1	0.5	0.1	0.1	1	0.210663	0.530379	−4.715725
1.0	1.0	0.2	0.5	0.1	0.1	1	0.206200	0.464706	−5.049206
1.0	1.0	0.3	0.5	0.1	0.1	1	0.213054	0.399379	−4.478912
1.0	1.0	0.1	0.6	0.1	0.1	1	0.308832	0.499116	−6.186873
1.0	1.0	0.1	0.8	0.1	0.1	1	0.089149	0.269012	−0.274342
1.0	1.0	0.1	0.1	0.2	0.1	1	0.172408	0.597149	−5.317236
1	1.0	0.1	0.1	0.3	0.1	1	0.143311	0.667716	−4.979897
1	1.0	0.1	0.1	0.1	0.2	1	0.200342	0.439178	−5.593338
1	1.0	0.1	0.1	0.1	0.3	1	−0.201322	0.337353	−5.563586
1	1.0	0.1	0.1	0.1	0.1	2	0.101483	0.507002	−6.155031
1	1.0	0.1	0.1	0.1	0.1	3	−0.130053	0.406443	3.655081

5.2 Graphical Results

5.2.1 Velocity Profiles

The influences of varying the thermophysical parameters on the velocity profiles for non-Newtonian Casson fluid are shown in Figures 2-16. The far-field boundary condition is satisfied when the fluid's velocity is minimal at the plate surface and increases to the free stream. The impact of the suction parameter (fw), the surface magnetic parameter (M_s) and bulk magnetic parameters on the velocity profiles are presented in Figures 10, 13, and 16, respectively. The combined effect of (M_s), (M_b), and fw decelerate the velocity. This is because the transverse magnetic field normal to the flow direction induces drag-like forces called the Lorentz forces which supply opposition to the fluid flow and suction too is an agent to the resistance of fluid flow and consequently decreases the fluid velocity. The effect of the Casson-like order (ω) and the Casson parameter (β) on the velocity profiles are illustrated in Figures 3 and 4. It is evident in the figures that enhancing both parameters decrease the velocity. This is because, improving the values of the parameters, increases the plastic dynamic viscosity that produces resistance in the fluid flow and hence a decrease in fluid velocity. It is noted from Figure 2 and 14 that increasing the values of the Grashof parameters tend to increase the buoyancy forces and the velocity at the surface. Meanwhile, increasing the angle of inclination (α) increases the velocity of the fluid flow as shown in Figure 15. This can be attributed to the fact that increasing the angle makes the surface steeper and almost vertical hence the increase in the flow velocity at the surface of the plate. We can note here that, increasing the angle of inclination of the surface will lead to improved stream kinematics.
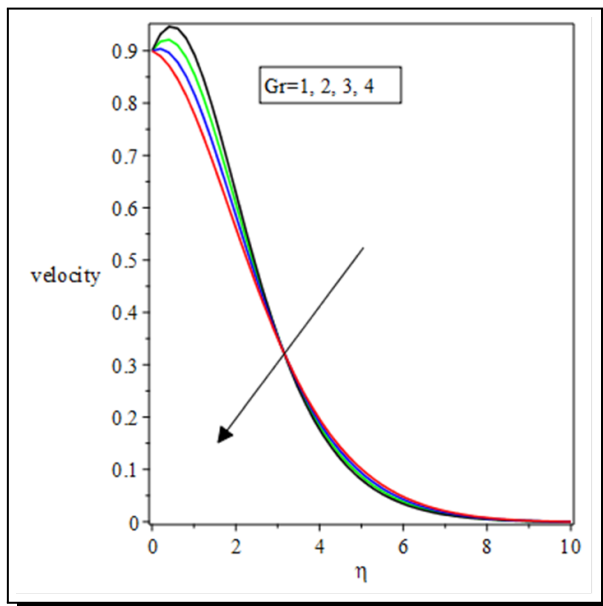
Figure 2. Velocity profiles for varying values of Gr for Pr = 0.72, λ = 0.1, Br = 1, α = 30, Ra = 0.1, m = 1, β = 1, Sc = 0.5, fw = 0.1, Gm = 1, M_b = 1, M_s = 0.1, ω = 1 and Q = 0.1
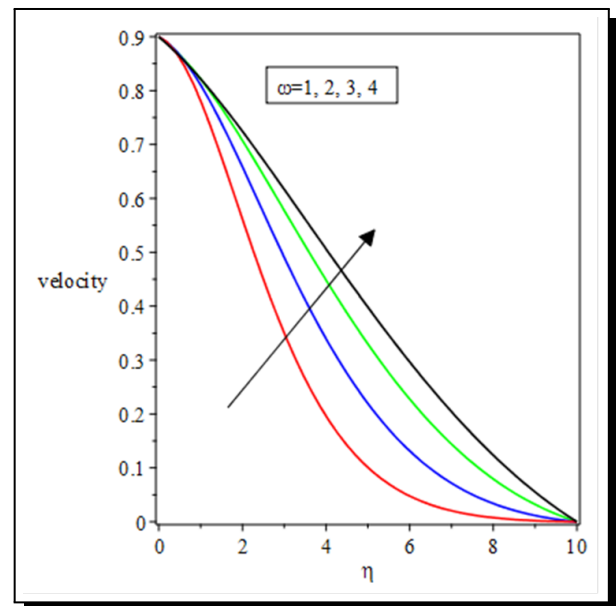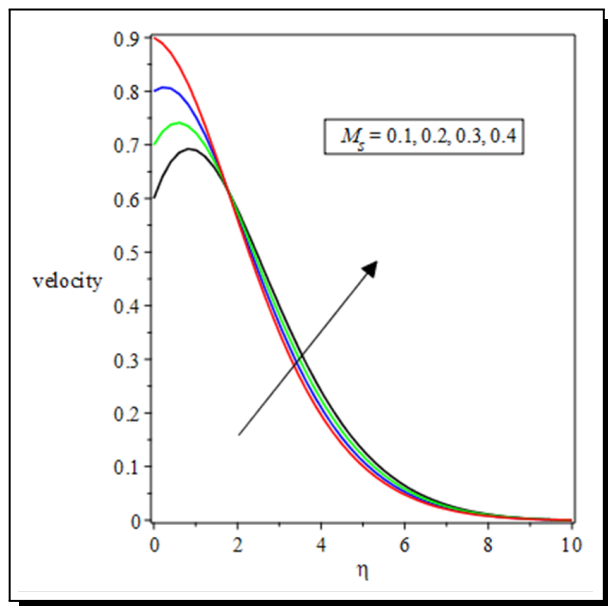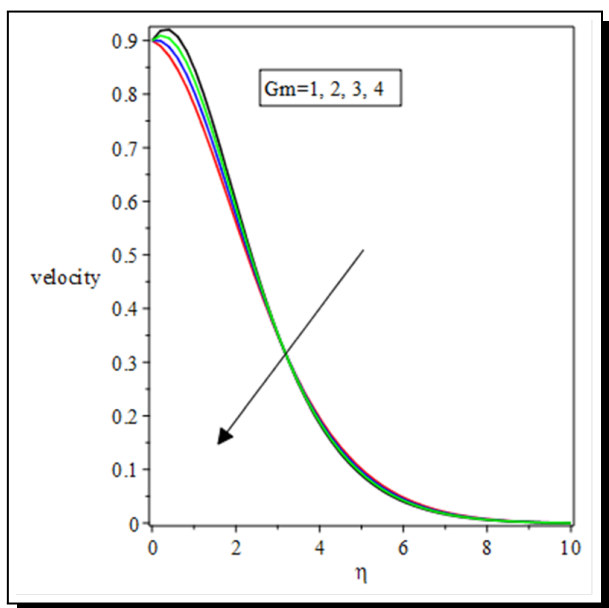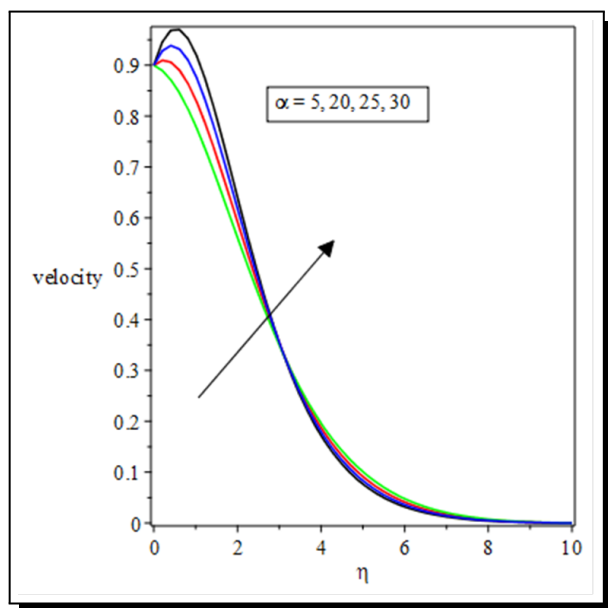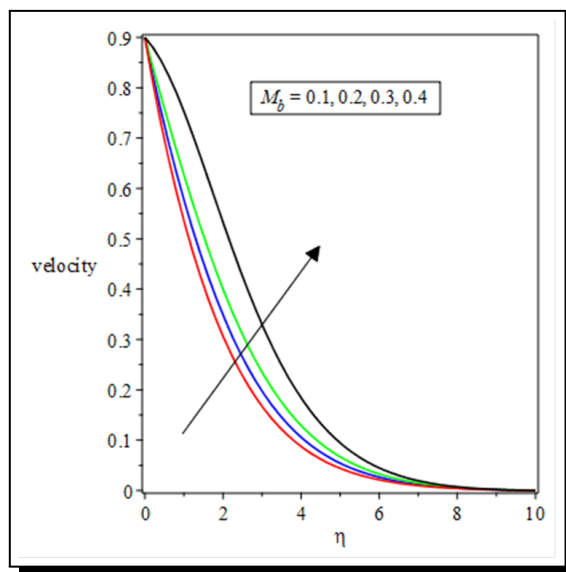
Figure 3. Velocity profiles for varying values of ω for Pr = 0.72, λ = 0.1, Br = 1, α = 30, Ra = 0.1, m = 1, β = 1, Sc = 0.5, fw = 0.1, Gr = 1, Gm = 1, M_b = 1, M_s = 0.1 and Q = 0.1
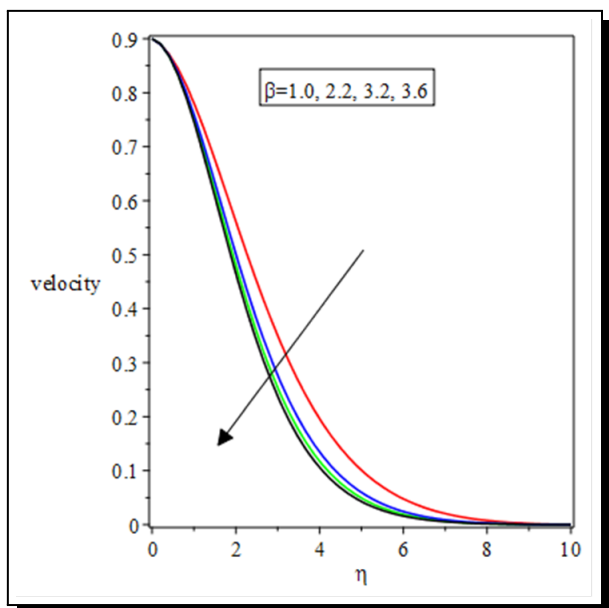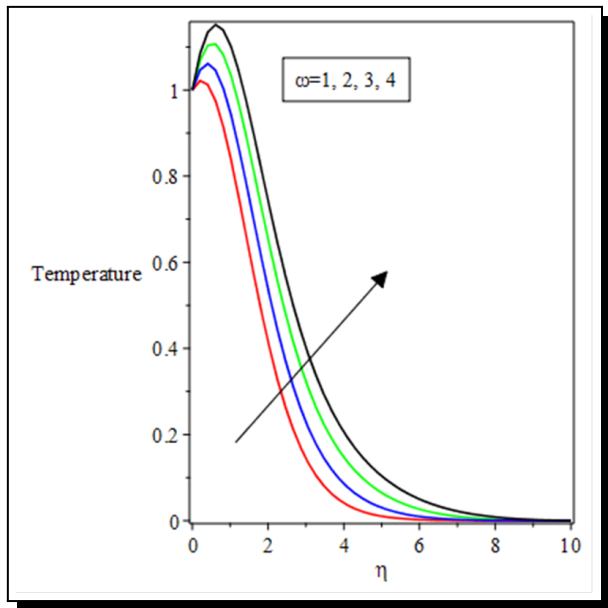
Figure 4. Velocity profiles for varying values of β for Pr = 0.72, λ = 0.1, Br = 1, α = 30, Ra = 0.1, m = 1, Sc = 0.5, fw = 0.1, Gr = 1, Gm = 1, M_b = 1, M_s = 0.1, ω = 1 and Q = 0.1
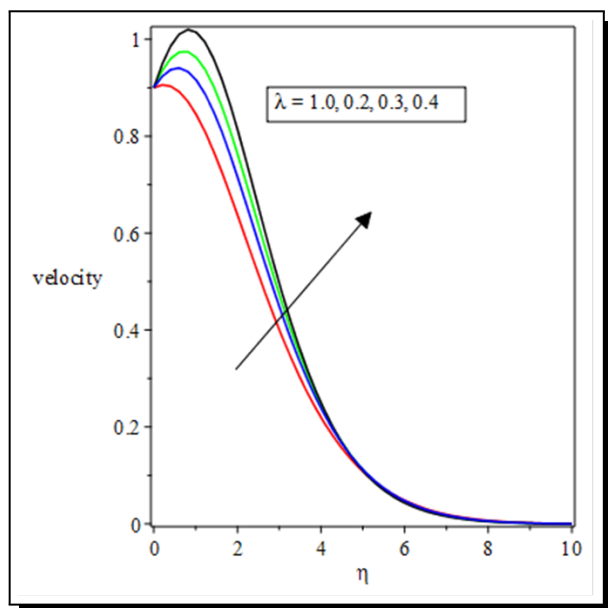
Figure 5. Velocity profiles for varying values of λ for Pr = 0.72, Br = 1, α = 30, Ra = 0.1, m = 1, β = 1, Sc = 0.5, fw = 0.1, Gr = 1, Gm = 1, M_b = 1, M_s = 0.1, ω = 1 and Q = 0.1
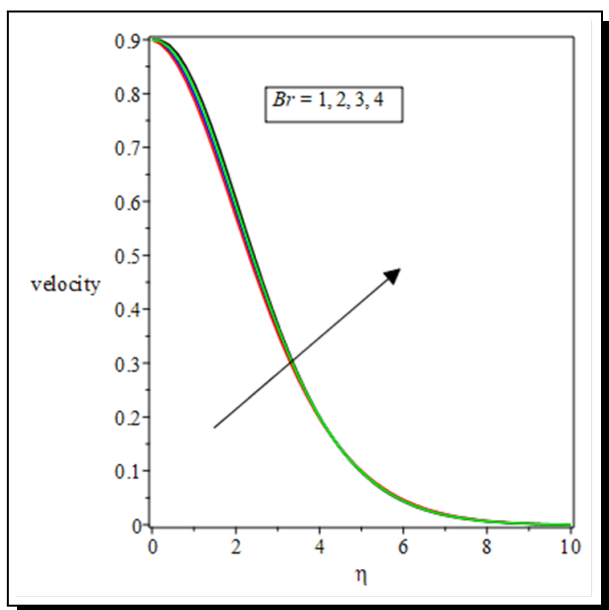
Figure 6. Velocity profiles for varying values of Br for Pr = 0.72, λ = 0.1, α = 30, Ra = 0.1, m = 1, β = 1, Sc = 0.5, fw = 0.1, Gr = 1, Gm = 1, M_b = 1, M_s = 0.1, ω = 1 and Q = 0.1
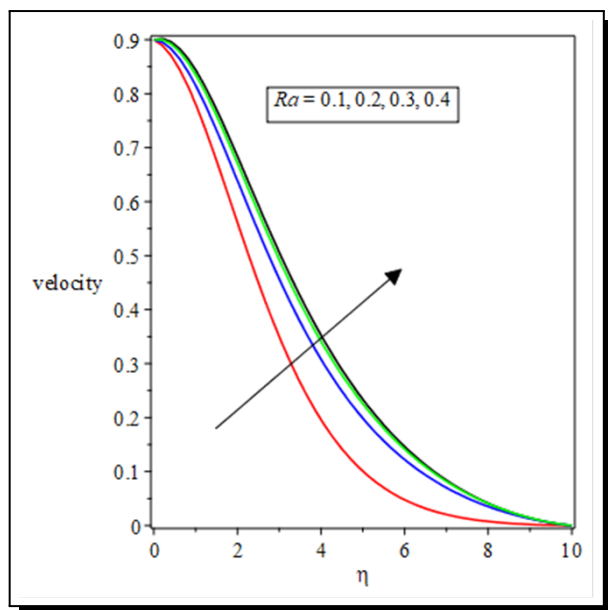
Figure 7. Velocity profiles for varying values of Ra for Pr = 0.72, λ = 0.1, Br = 1, α = 30, Ra = 0.1, m = 1, β = 1, Sc = 0.5, fw = 0.1, Gr = 1, Gm = 1, M_b = 1, M_s = 0.1, ω = 1 and Q = 0.1
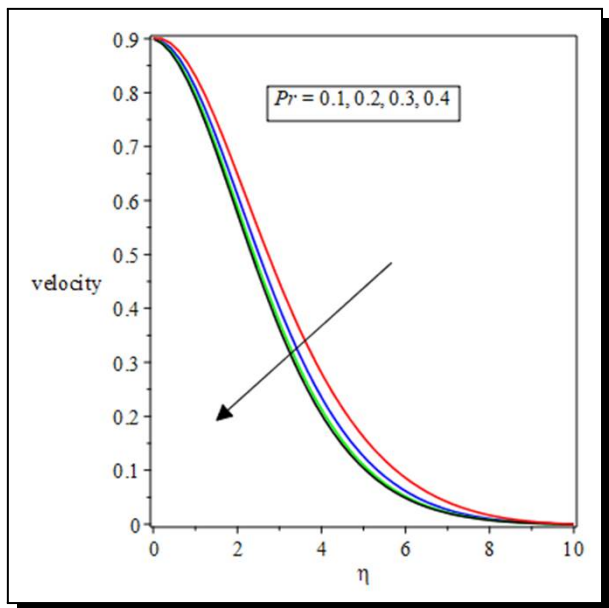
Figure 8. Velocity profiles for varying values of Pr for $\lambda = 0.1$, Br $= 1$, $\alpha = 30$, Ra $= 0.1$, $m = 1$, $\beta = 1$, Sc $= 0.5$, fw $= 0.1$, Gr $= 1$, Gm $= 1$, $M_b = 1$, $M_s = 0.1$, $\omega = 1$ and $Q = 0.1$
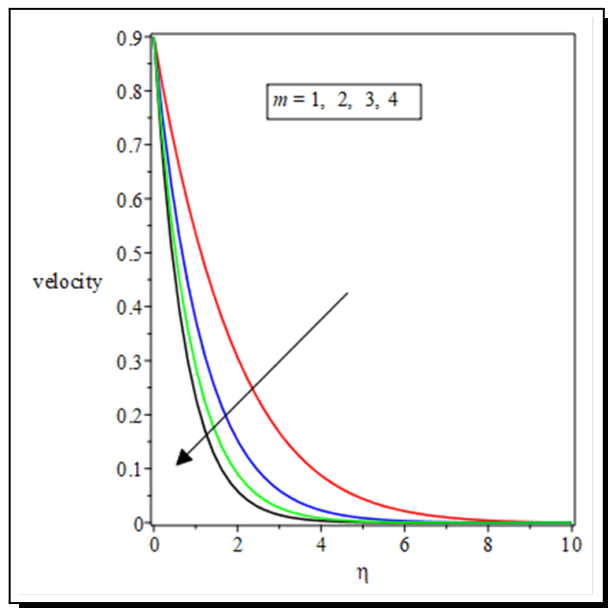
Figure 9. Velocity profiles for varying values of m for Pr $= 0.72$, $\lambda = 0.1$, Br $= 1$, $\alpha = 30$, Ra $= 0.1$, $\beta = 1$, Sc $= 0.5$, fw $= 0.1$, Gr $= 1$, Gm $= 1$, $M_b = 1$, $M_s = 0.1$, $\omega = 1$ and $Q = 0.1$
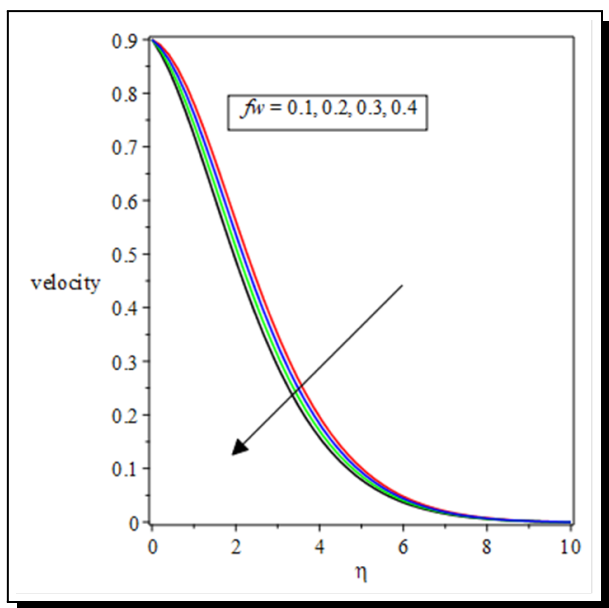
Figure 10. Velocity profiles for varying values of fw for Pr $= 0.72$, $\lambda = 0.1$, Br $= 1$, $\alpha = 30$, Ra $= 0.1$, $\beta = 1$, $m = 1$, fw $= 0.1$, Gr $= 1$, Gm $= 1$, $M_b = 1$, $M_s = 0.1$, $\omega = 1$ and $Q = 0.1$
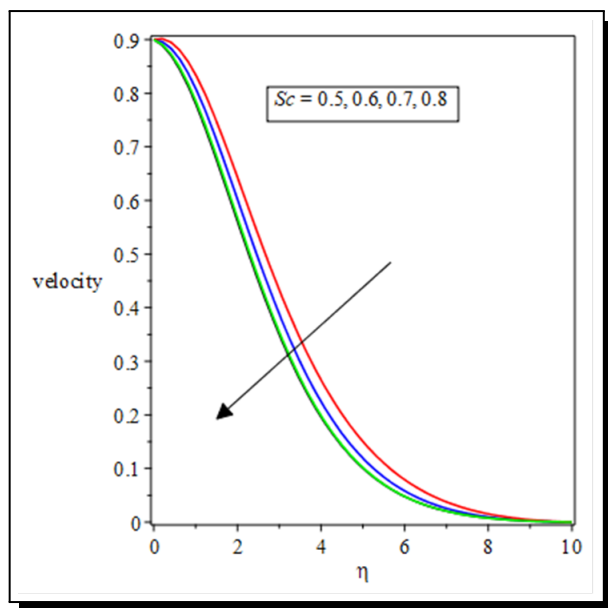
Figure 11. Velocity profiles for varying values of Sc for Pr $= 0.72$, $\lambda = 0.1$, Br $= 1$, $\alpha = 30$, Ra $= 0.1$, $m = 1$, $\beta = 1$, fw $= 0.1$, Gr $= 1$, Gm $= 1$, $M_b = 1$, $M_s = 0.1$, $\omega = 1$ and $Q = 0.1$
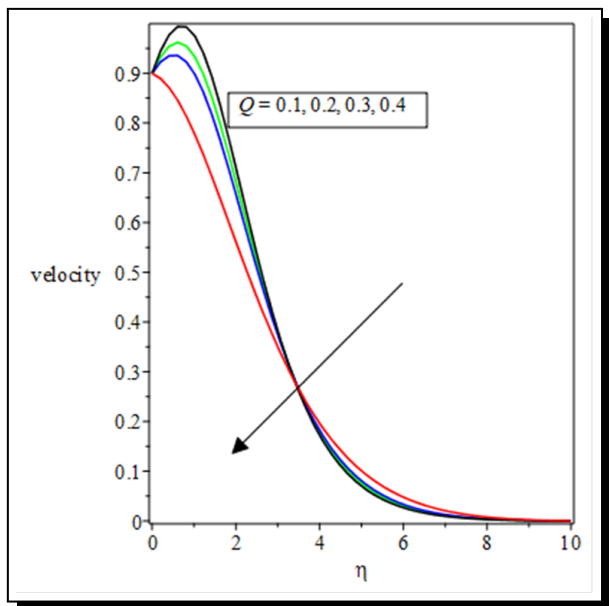
Figure 12. Velocity profiles for varying values of Q for Pr = 0.72, $\lambda = 0.1$, Br = 1, $\alpha = 30$, Ra = 0.1, $m = 1$, $\beta = 1$, Sc = 0.5, fw = 0.1, Gr = 1, Gm = 1, $M_b = 1$, $M_s = 0.1$ and $\omega = 1$

Figure 13. Velocity profiles for varying values of M_s for Pr = 0.72, $\lambda = 0.1$, Br = 1, $\beta = 30$, Ra = 0.1, $m = 1$, $\beta = 1$, Sc = 0.5, fw = 0.1, Gr = 1, Gm = 1, $M_b = 1$, $\omega = 1$ and $Q = 0.1$

Figure 14. Velocity profiles for varying values of Gm for Pr = 0.72, $\lambda = 0.1$, Br = 1, $\alpha = 30$, Ra = 0.1, $m = 1$, $\beta = 1$, Sc = 0.5, fw = 0.1, Gr = 1, $M_b = 1$, $M_s = 0.1$, $\omega = 1$ and $Q = 0.1$

Figure 15. Velocity profiles for varying values of α for Pr = 0.72, $\lambda = 0.1$, Br = 1, Ra = 0.1, $m = 1$, $\beta = 1$, Sc = 0.5, fw = 0.1, Gr = 1, Gm = 1, $M_b = 1$, $M_s = 0.1$, $\omega = 1$ and $Q = 0.1$
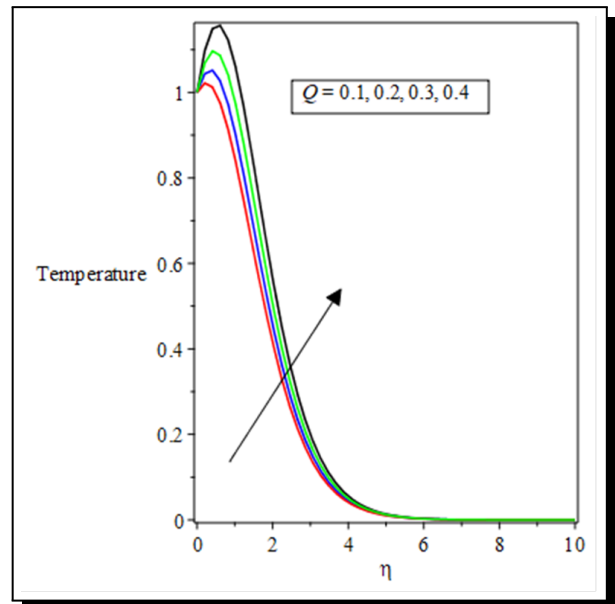
Figure 16. Velocity profiles for varying values of M_b for Pr = 0.72, λ = 0.1, Br = 1, α = 30, Ra = 0.1, m = 1, β = 1, Sc = 0.5, fw = 0.1, Gr = 1, Gm = 1, M_s = 0.1, ω = 1 and Q = 0.1

5.2.2 Temperature Profiles

The effects of parameter variation on temperature profiles are shown in Figures 17-32. Figure 19 shows how the Prandtl number affects the temperature of the fluid. Since the Prandtl number is the ratio of the momentum diffusivity to the thermal diffusivity then an increase in the Prandtl number implies a decrease in the thermal diffusivity or increase in the momentum diffusivity. Consequently, as the Prandtl number increases, convection becomes more responsible for the transfer of energy than heat diffusion. Thus, it reduces the thickness of the thermal boundary layer therefore heat diffuses out faster from the sheet. So the thinner the thermal boundary layer becomes the decrease in temperature. In Figures 26 and 31, the effects of the surface and bulk magnetic field parameters on temperature profiles are illustrated. The magnetic effect causes skin-frictional heating and so the wall temperature increases and the thickness of the thermal boundary layer increases.

The effect of the reaction rate parameter (λ) on temperature profile is shown in Figure 27. The thermal boundary-layer thickness decreases with increasing the reaction rate parameter. It is observed in Figure 21 that, increasing fw also reduces the temperature profile for obvious reasons. Figure 28 indicates that thermal radiation (Ra) increases the temperature profiles. This is because, as more heat is generated within the fluid, the fluid temperature increases leading to a sharp inclination of the temperature gradient between the plate surface and the fluid.

The effect of heat source parameter Q on the temperature profile is shown in Figure 20. From the figure, we found that the heat source parameter Q increases the conductivity of the fluid and the thickening of the thermal boundary layer. This shows that the thermal boundary layer thickness increases with an increase of the heat source parameter Q. Figure 18 shows the influence of viscous dissipation parameter Br on the temperature profile. Thus, as it is visible from the figure, we observed that increasing the viscous dissipation parameter Br increases the temperature profile. This shows that the thermal boundary layer thickness increases with an increase of viscous dissipation parameter Br. This is because the energy stored in the fluid region is a consequence of dissipation, viscosity, and elastically deforms.

Figure 17. Temperature profiles for varying values of ω for $Pr = 0.72$, $\lambda = 0.1$, $Br = 1$, $\alpha = 30$, $Ra = 0.1$, $m = 1$, $\beta = 1$, $Sc = 0.5$, $fw = 0.1$, $Gr = 1$, $M_b = 1$, $M_s = 0.1$, $Gm = 1$ and $Q = 0.1$
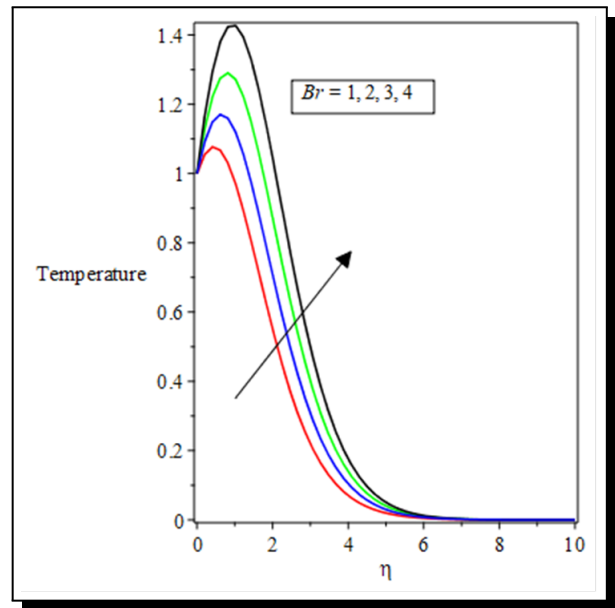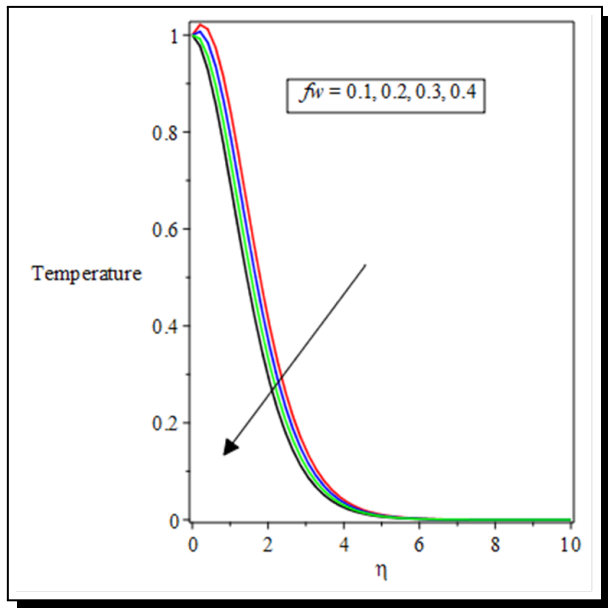

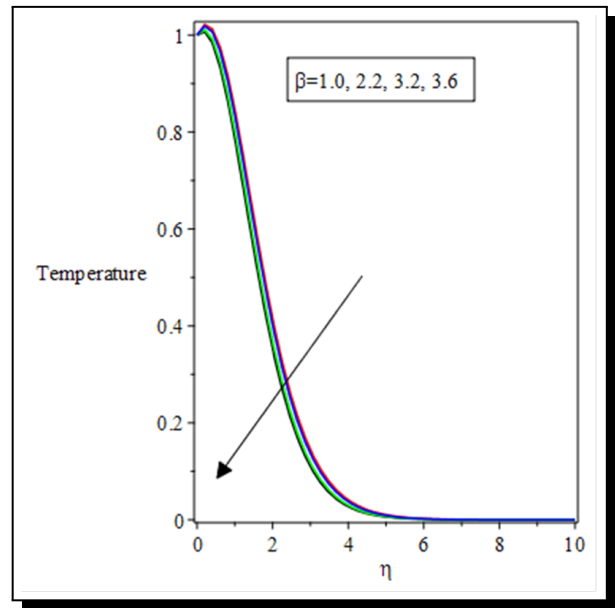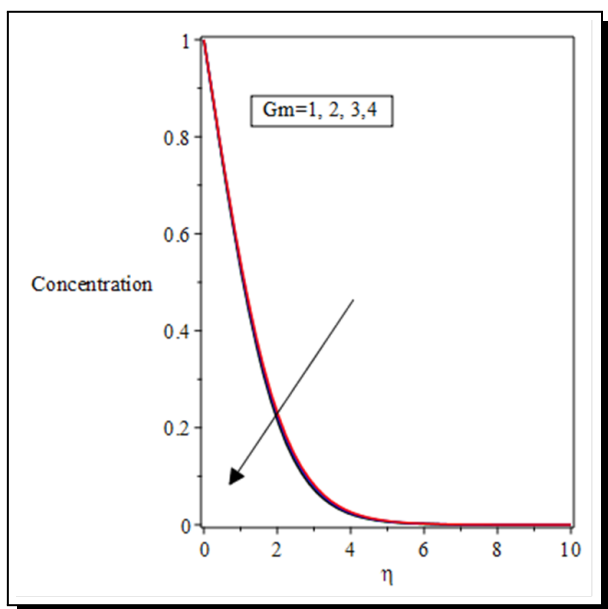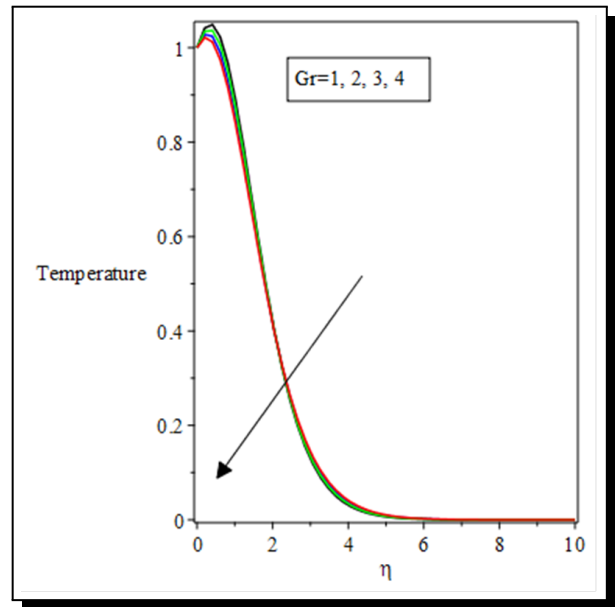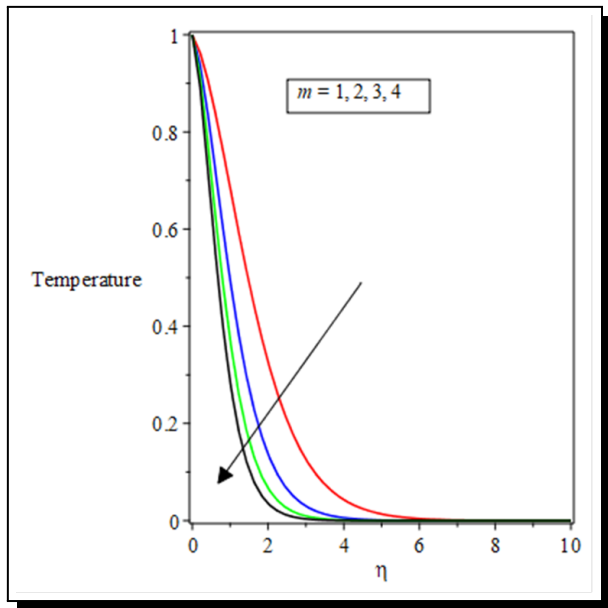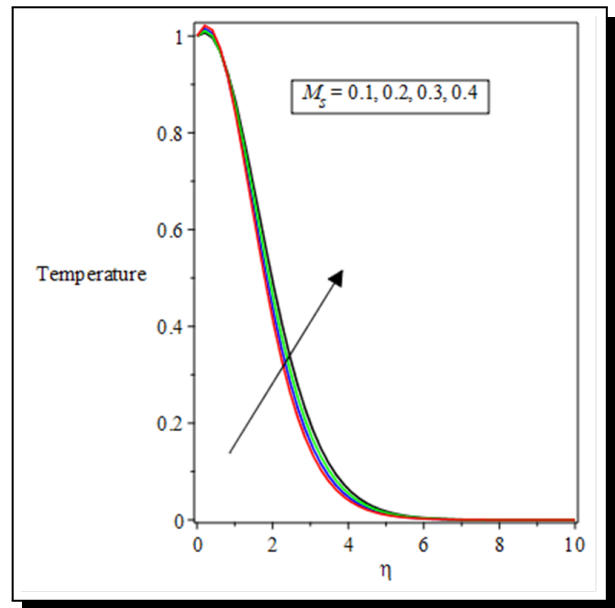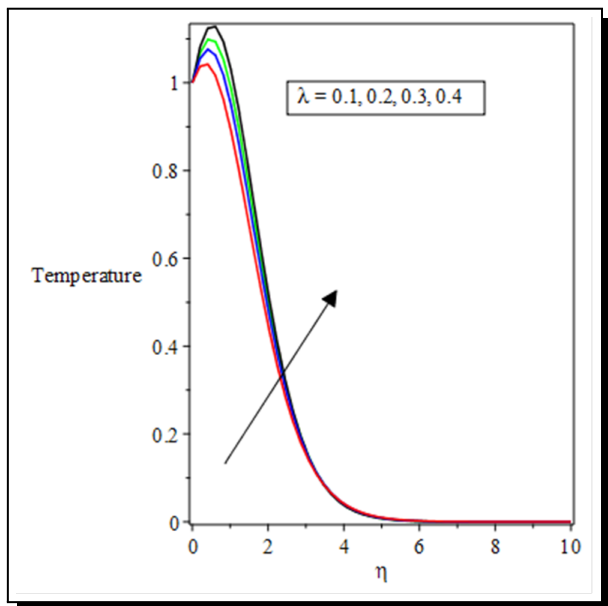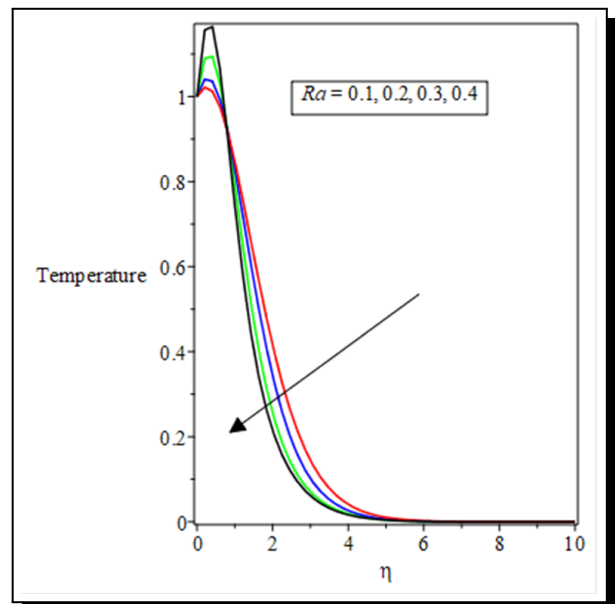**Figure 18.** Temperature profiles for varying values of Br for $Pr = 0.72$, $\lambda = 0.1$, $\alpha = 30$, $Ra = 0.1$, $m = 1$, $\beta = 1$, $Sc = 0.5$, $fw = 0.1$, $Gr = 1$, $M_b = 1$, $M_s = 0.1$, $Gm = 1$, $\omega = 1$ and $Q = 0.1$
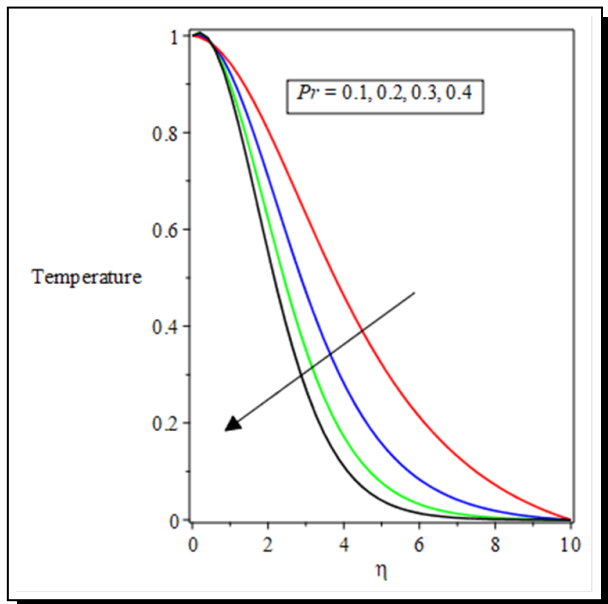
Figure 19. Temperature profiles for varying values of Pr for $\lambda = 0.1$, $Br = 1$, $\alpha = 30$, $Ra = 0.1$, $m = 1$, $\beta = 1$, $Sc = 0.5$, $fw = 0.1$, $Gr = 1$, $M_b = 1$, $M_s = 0.1$, $Gm = 1$, $\omega = 1$ and $Q = 0.1$
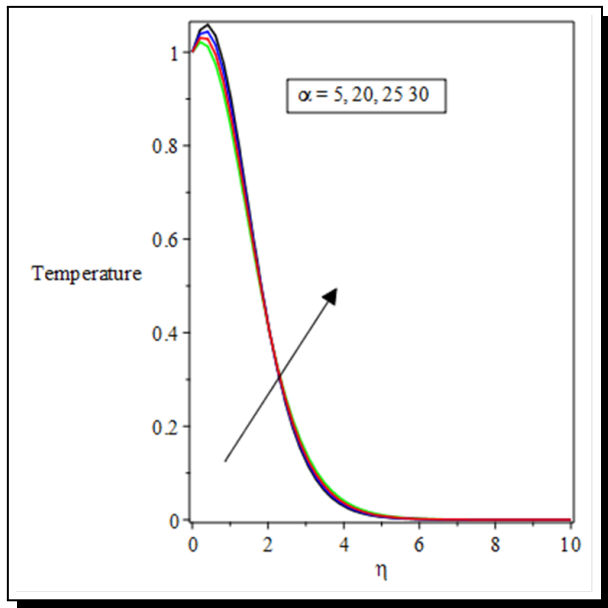

Figure 20. Temperature profiles for varying values of Q for $Pr = 0.72$, $\lambda = 0.1$, $Br = 1$, $\alpha = 30$, $Ra = 0.1$, $m = 1$, $\beta = 1$, $Sc = 0.5$, $fw = 0.1$, $Gr = 1$, $M_b = 1$, $M_s = 0.1$, $Gm = 1$ and $\omega = 1$
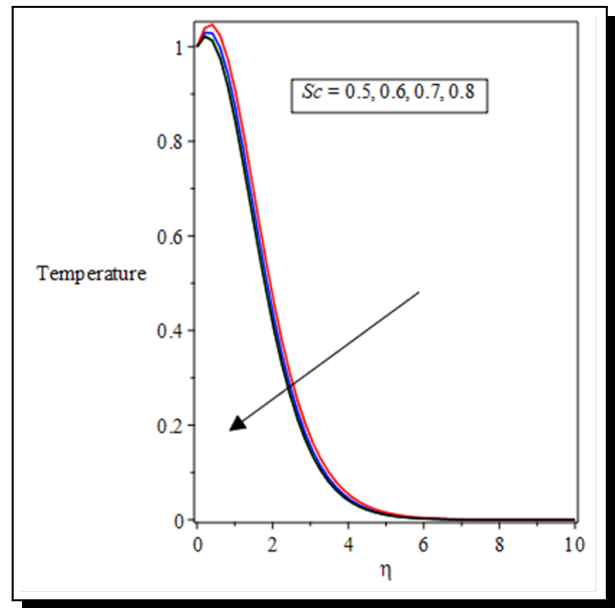
Figure 21. Temperature profiles for varying values of fw for Pr = 0.72, $\lambda = 0.1$, Br = 1, $\alpha = 30$, Ra = 0.1, $m = 1$, $\beta = 1$, Sc = 0.5, Gr = 1, $M_b = 1$, $M_s = 0.1$, Gm = 1, $\omega = 1$ and $Q = 0.1$

Figure 22. Temperature profiles for varying values of λ for Pr = 0.72, $\alpha = 0.1$, Br = 1, $\beta = 30$, Ra = 0.1, $m = 1$, Sc = 0.5, fw = 0.1, Gr = 1, $M_b = 1$, $M_s = 0.1$, Gm = 1, $\omega = 1$ and $Q = 0.1$
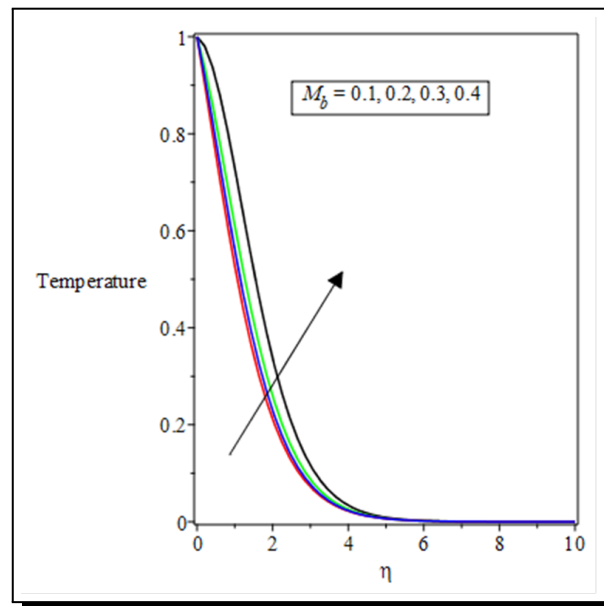

Figure 23. Temperature profiles for varying values of Gm for Pr = 0.72, $\lambda = 0.1$, Br = 1, $\alpha = 30$, Ra = 0.1, $m = 1$, $\beta = 1$, Sc = 0.5, fw = 0.1, Gr = 1, $M_b = 1$, $M_s = 0.1$, $\omega = 1$ and $Q = 0.1$

Figure 24. Temperature profiles for varying values of Gr for Pr = 0.72, $\lambda = 0.1$, Br = 1, $\alpha = 30$, Ra = 0.1, $m = 1$, $\beta = 1$, Sc = 0.5, fw = 0.1, $M_b = 1$, $M_s = 0.1$, Gm = 1, $\omega = 1$ and $Q = 0.1$

Figure 25. Temperature profiles for varying values of m for Pr = 0.72, $\lambda = 0.1$, Br = 1, $\alpha = 30$, Ra = 0.1, $\beta = 1$, Sc = 0.5, fw = 0.1, Gr = 1, $M_b = 1$, $M_s = 0.1$, Gm = 1, $\omega = 1$ and $Q = 0.1$

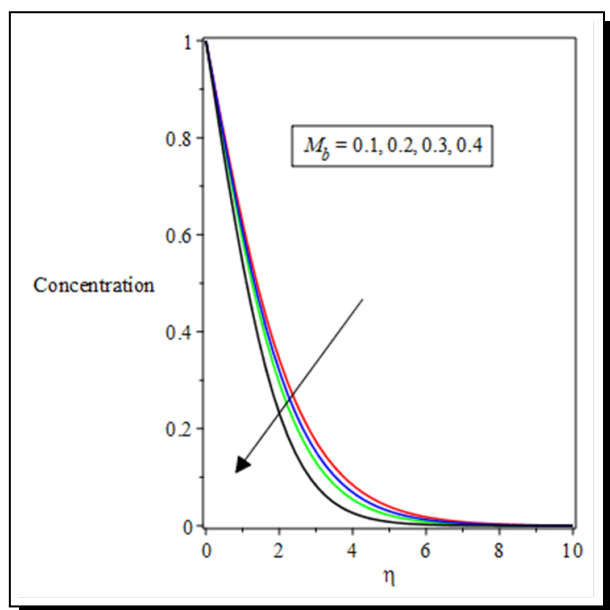**Figure 26.** Temperature profiles for varying values of M_s for Pr = 0.72, $\lambda = 0.1$, Br = 1, $\alpha = 30$, Ra = 0.1, $m = 1$, $\beta = 1$, Sc = 0.5, fw = 0.1, Gr = 1, $M_b = 1$, Gm = 1, $\omega = 1$ and $Q = 0.1$

Figure 27. Temperature profiles for varying values of λ for Pr = 0.72, Br = 1, $\alpha = 30$, Ra = 0.1, $m = 1$, $\beta = 1$, Sc = 0.5, fw = 0.1, Gr = 1, $M_b = 1$, $M_s = 0.1$, Gm = 1, $\omega = 1$ and $Q = 0.1$


Figure 28. Temperature profiles for varying values of Ra for Pr = 0.72, $\lambda = 0.1$, Br = 1, $\alpha = 30$, $m = 1$, $\beta = 1$, Sc = 0.5, fw = 0.1, Gr = 1, $M_b = 1$, $M_s = 0.1$, Gm = 1, $\omega = 1$ and $Q = 0.1$

Figure 29. Temperature profiles for varying values of α for Pr = 0.72, λ = 0.1, Br = 1, Ra = 0.1, m = 1, β = 1, Sc = 0.5, fw = 0.1, Gr = 1, M_b = 1, M_s = 0.1, Gm = 1, ω = 1 and Q = 0.1

Figure 30. Temperature profiles for varying values of Sc for Pr = 0.72, λ = 0.1, Br = 1, α = 30, Ra = 0.1, m = 1, β = 1, fw = 0.1, Gr = 1, M_b = 1, M_s = 0.1, Gm = 1, ω = 1 and Q = 0.1

Figure 31. Temperature profiles for varying values of M_b for Pr = 0.72, λ = 0.1, Br = 1, α = 30, Ra = 0.1, m = 1, β = 1, Sc = 0.5, fw = 0.1, Gr = 1, M_s = 0.1, Gm = 1, ω = 1 and Q = 0.1

5.2.3 Concentration Profiles

Figures 32-46 present the plots of concentration profiles for non-Newtonian Casson fluid for varying values of the emerged thermophysical parameters. The effect of bulk magnetic parameter (M_b), surface magnetic parameter (M_s) and both the Cason parameter (β) and its order (ω) are observed in Figures 32, 41, 46 and 43, respectively. It is noteworthy that by increasing the surface magnetic parameter, the bulk magnetic parameter, and the Casson parameter, the concentration boundary layer thickness increases. It is observed from Figures4 and 46 that the Casson parameter β has quite opposite effects on the velocity and concentration profiles. In the same manner, the buoyancy force due to species concentration is also triggered by increasing values of Gm to reduce the concentration boundary layer thickness as shown in Figure 35.

Figure 40 depicts that the concentration boundary layer thickness decreases with increasing values of Sc. In practice, increasing Schmidt number means increasing momentum diffusion over mass diffusion which in turn reduces the concentration profile. At a point in the flow where λ is zero implies no chemical reaction. On the other hand, an increase in λ means an increase in the chemical reaction rate which causes a reduction in concentration. Figure 39 affirms this since it can be seen that increasing values of λ decreases the concentration boundary layer thickness. Moreover, it is observed in Figure 42 that increasing the values of fw has an adverse effect of decaying the concentration boundary layer thickness.
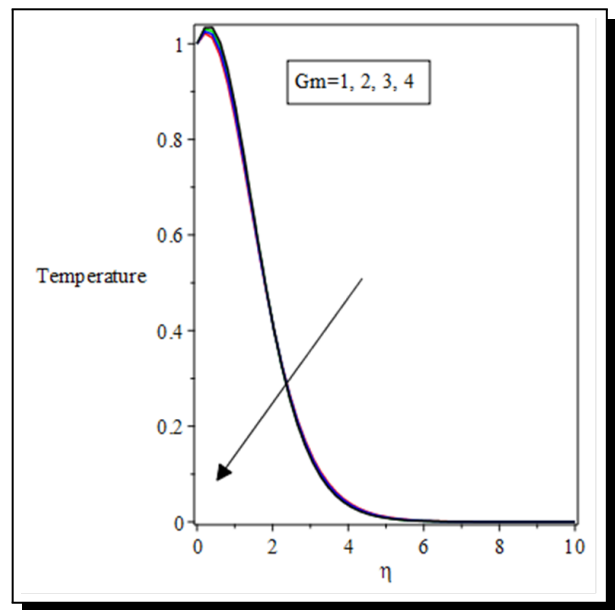
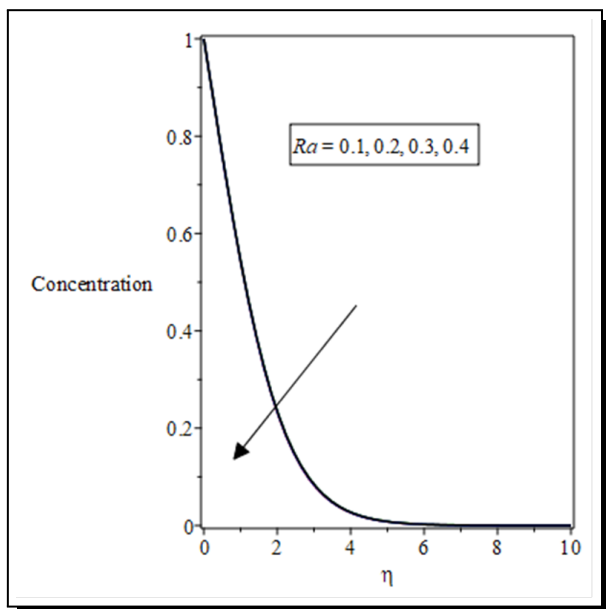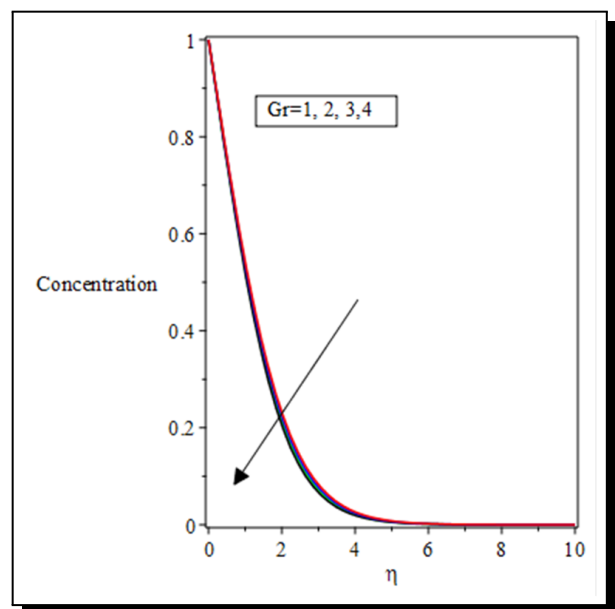

Figure 32. Concentration profiles for varying values of M_b for Pr = 0.72, $\lambda = 0.1$, Br = 1, $\alpha = 30$, Ra = 0.1, $m = 1$, $\beta = 1$, Sc = 0.5, fw = 0.1, Gr = 1, Gm = 1, $M_s = 0.1$, $\omega = 1$ and $Q = 0.1$
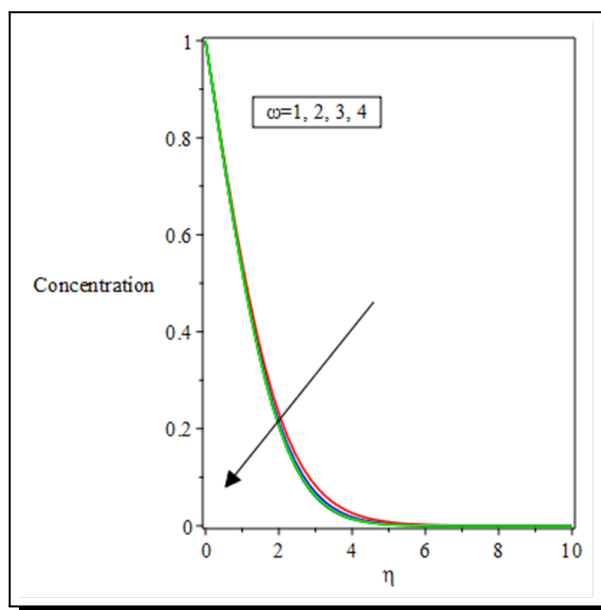
Figure 33. Concentration profiles for varying values of ω for Pr = 0.72, $\lambda = 0.1$, Br = 1, $\alpha = 30$, Ra = 0.1, $m = 1$, $\beta = 1$, Sc = 0.5, fw = 0.1, Gr = 1, Gm = 1, $M_b = 1$, $M_s = 0.1$ and $Q = 0.1$
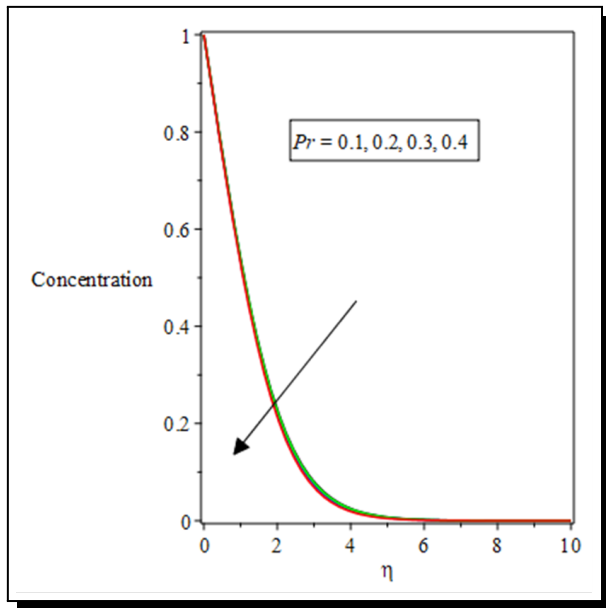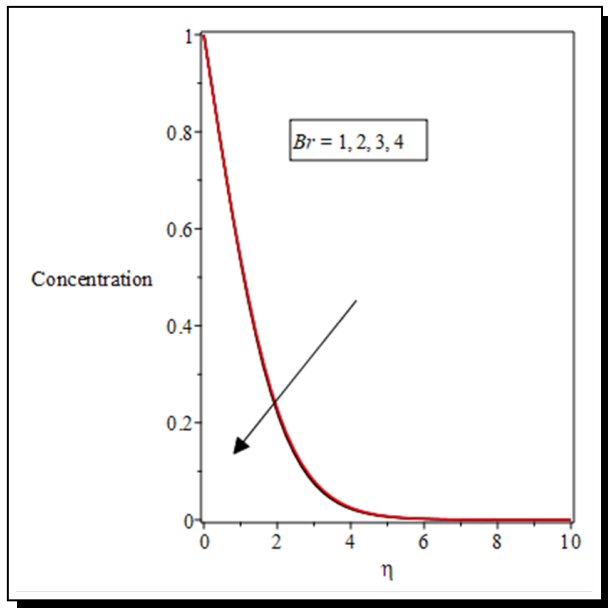
Figure 34. Concentration profiles for varying values of Pr for Pr = 0.72, λ = 0.1, Br = 1, α = 30, Ra = 0.1, m = 1, β = 1, Sc = 0.5, fw = 0.1, Gr = 1, Gm = 1, M_b = 1, M_s = 0.1, ω = 1 and Q = 0.1

Figure 35. Concentration profiles for varying values of Gm for Pr = 0.72, λ = 0.1, Br = 1, α = 30, Ra = 0.1, m = 1, β = 1, Sc = 0.5, fw = 0.1, Gr = 1, M_b = 1, M_s = 0.1, ω = 1 and Q = 0.1

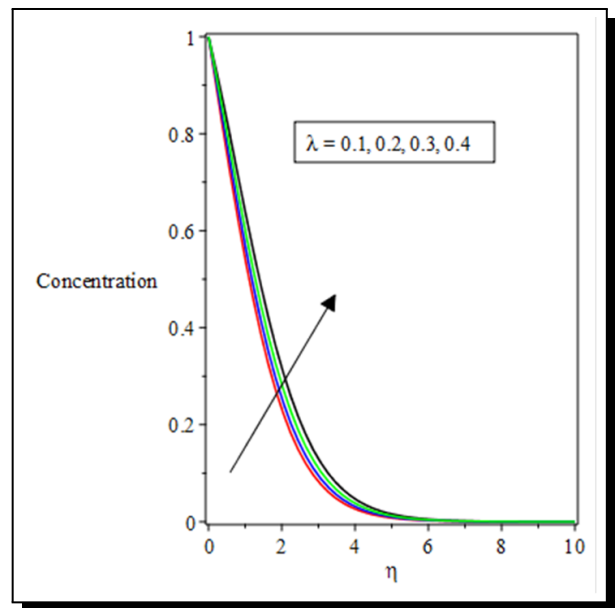
Figure 36. Concentration profiles for varying values of Ra for Pr = 0.72, λ = 0.1, Br = 1, α = 30, m = 1, β = 1, Sc = 0.5, fw = 0.1, Gr = 1, Gm = 1, M_b = 1, M_s = 0.1, ω = 1 and Q = 0.1
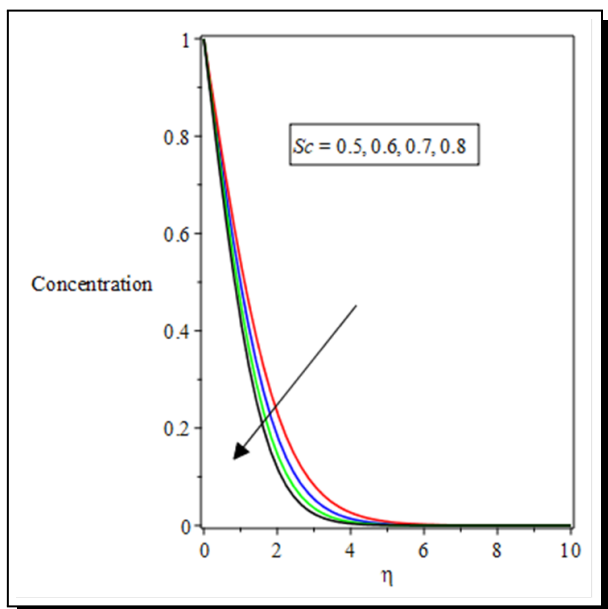

Figure 37. Concentration profiles for varying values of Gr for Pr = 0.72, λ = 0.1, Br = 1, α = 30, Ra = 0.1, m = 1, β = 1, Sc = 0.5, fw = 0.1, Gm = 1, M_b = 1, M_s = 0.1, ω = 1 and Q = 0.1
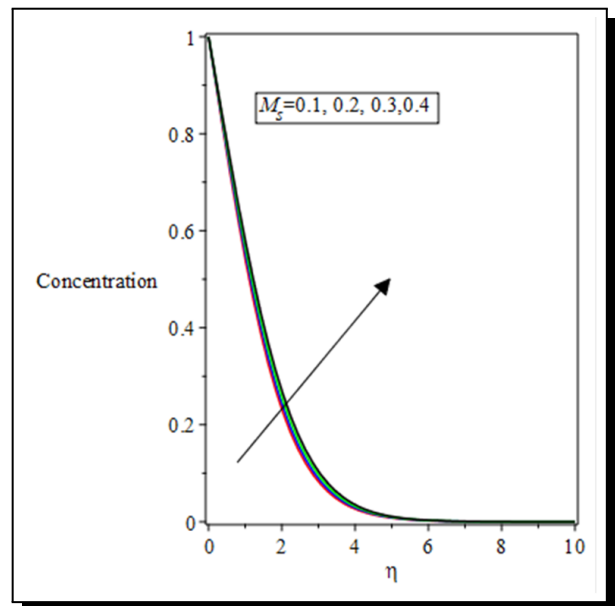
Figure 38. Concentration profiles for varying values of Br for Pr = 0.72, λ = 0.1, Br = 1, α = 30, Ra = 0.1, m = 1, β = 1, Sc = 0.5, fw = 0.1, Gr = 1, Gm = 1, M_b = 1, M_s = 0.1, ω = 1 and Q = 0.1
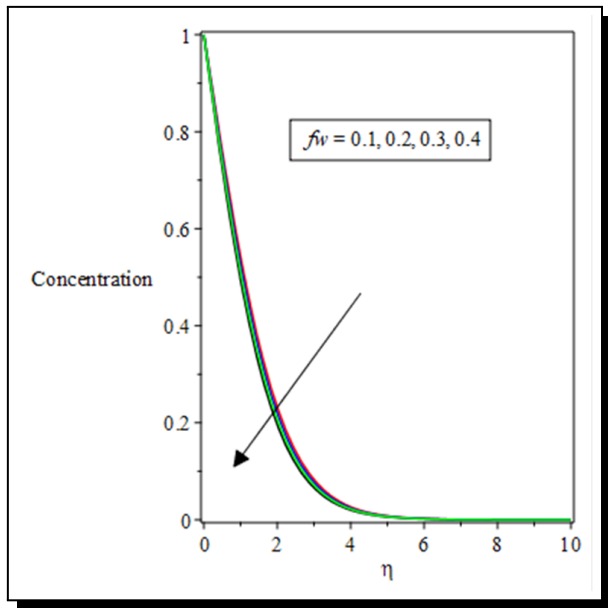

Figure 39. Concentration profiles for varying values of λ for Pr = 0.72, Br = 1, α = 30, Ra = 0.1, m = 1, β = 1, Sc = 0.5, fw = 0.1, Gr = 1, Gm = 1, M_b = 1, M_s = 0.1, ω = 1 and Q = 0.1

Figure 40. Concentration profiles for varying values of Sc for Pr = 0.72, λ = 0.1, Br = 1, α = 30, Ra = 0.1, m = 1, β = 1, fw = 0.1, Gr = 1, Gm = 1, M_b = 1, M_s = 0.1, ω = 1 and Q = 0.1

Figure 41. Concentration profiles for varying values of M_s for Pr = 0.72, λ = 0.1, Br = 1, α = 30, Ra = 0.1, m = 1, β = 1, Sc = 0.5, fw = 0.1, Gr = 1, Gm = 1, M_s = 0.1, ω = 1 and Q = 0.1
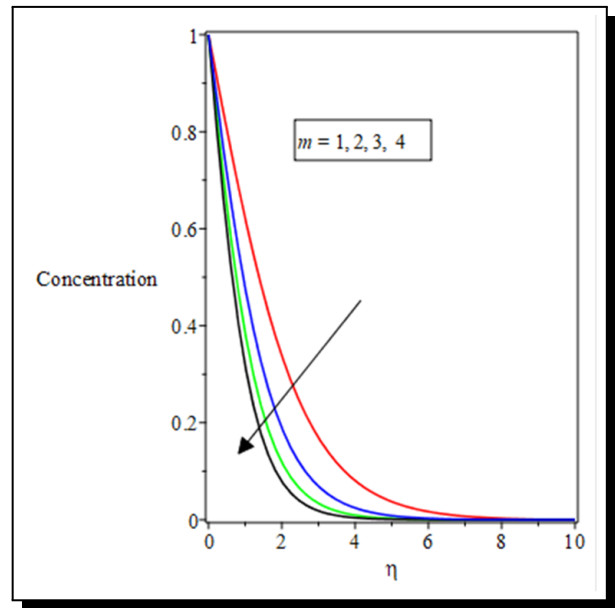
Figure 42. Concentration profiles for varying values of fw for Pr = 0.72, λ = 0.1, Br = 1, α = 30, Ra = 0.1, m = 1, β = 1, Sc = 0.5, Gr = 1, Gm = 1, M_b = 1, M_s = 0.1, ω = 1 and Q = 0.1

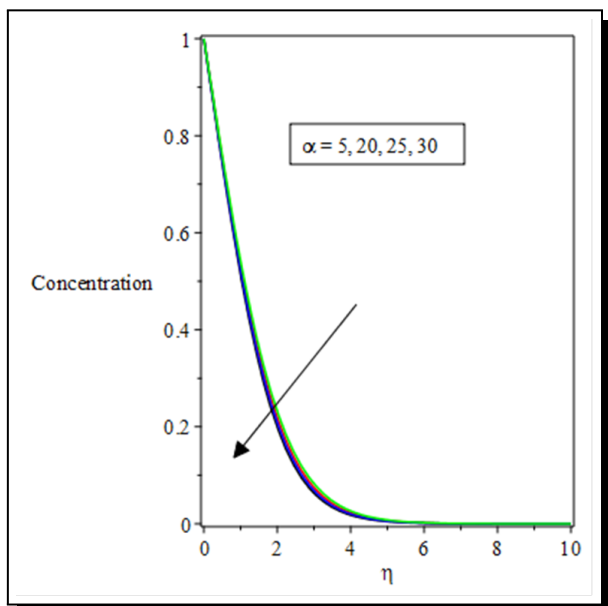**Figure 43.** Concentration profiles for varying values of m for Pr = 0.72, λ = 0.1, Br = 1, α = 30, Ra = 0.1, β = 1, Sc = 0.5, fw = 0.1, Gr = 1, Gm = 1, M_b = 1, M_s = 0.1, ω = 1 and Q = 0.1

Figure 44. Concentration profiles for varying values of α for Pr = 0.72, λ = 0.1, Br = 1, Ra = 0.1, m = 1, β = 1, Sc = 0.5, fw = 0.1, Gr = 1, Gm = 1, M_b = 1, M_s = 0.1, ω = 1 and Q = 0.1
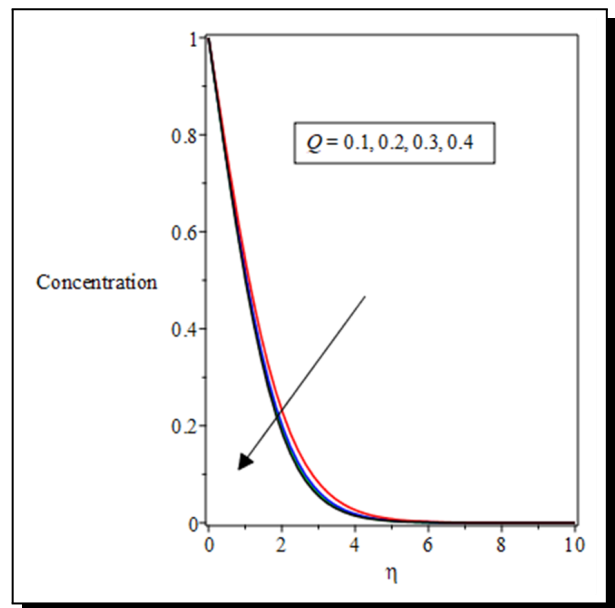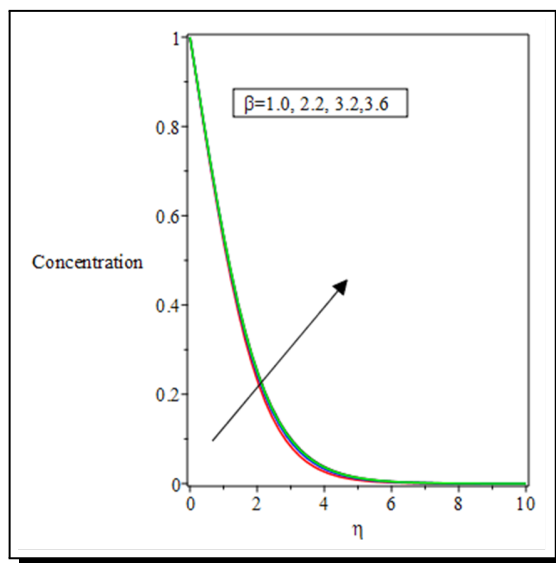

Figure 45. Concentration profiles for varying values of Q for Pr = 0.72, λ = 0.1, Br = 1, α = 30, Ra = 0.1, m = 1, β = 1, Sc = 0.5, fw = 0.1, Gr = 1, Gm = 1, M_b = 1, M_s = 0.1 and ω = 1

Figure 46. Concentration profiles for varying values of β for Pr = 0.72, λ = 0.1, Br = 1, α = 30, Ra = 0.1, m = 1, Sc = 0.5, fw = 0.1, Gr = 1, Gm = 1, M_b = 1, M_s = 0.1, ω = 1 and Q = 0.1

6. Conclusion

The effect of angle of inclination on Casson-like fluid flow with chemical reaction in the presence of a transverse magnetic field at the surface has been studied. Numerical results have been compared to earlier results published in the literature and a perfect agreement was achieved. Among others, our results reveal that proper control of the angle of inclination of the surface could lead to better flow kinematics.

7. Recommendations

Manufacturing and engineering processes should incorporate magnetized surfaces to improve the cooling or heating processes. The heat generation can be controlled through modulation of the magnetization strength at the bulk surfaces.

Competing Interests
The authors declare that they have no competing interests.

Authors' Contributions
All the authors contributed significantly in writing this article. The authors read and approved the final manuscript.

References

[1] A.A. Afify, The influence of slip boundary condition on Casson nanofluid flow over a stretching sheet in the presence of viscous dissipation and chemical reaction, *Mathematical Problems in Engineering* **2017** (2017), 12 pages, DOI: 10.1155/2017/3804751.

[2] G. Aloliga, Y.I. Seini and R. Musah, Heat transfer in a magnetohydrodynamic boundary layer flow of a non-Newtonian Casson fluid over an exponentially stretching magnetized surface, *Journal of Nanofluids* **10**(2) (2021), 172 – 185, DOI: 10.1166/jon.2021.1777.

[3] E.M. Arthur, G. Aloliga and I.Y. Seini, MHD Casson fluid flow over an inclined surface with suction and chemical reaction, *Asian Journal of Mathematics and Computer Research* **6** (4) (2015), 367 – 380, URL: https://www.ikprress.org/index.php/AJOMCOR/article/view/303.

[4] K. Bhattacharyya, T. Hayat and A. Alsaedi, Exact solution for boundary layer flow of Casson fluid over a permeable stretching/shrinking sheet, *ZAMM - Journal of Applied Mathematics and Mechanics* **94**(6), 522 – 528, DOI: 10.1002/zamm.201200031.

[5] N. Casson, A flow equation for pigment oil suspensions of the printing ink type, in: C.C. Mill (editor), *Rheology of Disperse Systems*, Pergamon Press, Oxford, pp. 84 – 102 (1959).

[6] N.T.M. Eldabe and M.G.E. Salwa, Heat transfer of MHD non-Newtonian Casson fluid flow between two rotating cylinders, *Journal of the Physical Society of Japan* **64** (1995), 41 – 46.

[7] T. Hayat, M.B. Ashraf, S.A. Shehzad and A. Alsaedi, Mixed convection flow of Casson nanofluid over a stretching sheet with convectively heated chemical reaction and heat source/sink, *Journal of Applied Fluid Mechanics* **8**(4) (2015), 803 – 811, DOI: 10.18869/acadpub.jafm.67.223.22995.

[8] T. Hayat, S.A. Shehzad, A. Alsaedi and M.S. Alhothuali, Mixed convection stagnation point flow of Casson fluid with convective boundary conditions, *Chinese Physics Letters* **29**(11) (2012), 114704, DOI: 10.1088/0256-307X/29/11/114704.

[9] A. Hussanan, M.Z. Salleh, R.M. Tahar and I. Khan, Unsteady boundary layer flow and heat transfer of a Casson fluid past an oscillating vertical plate with Newtonian heating, *PLOS ONE* **9**(10) (2014), e108763, DOI: 10.1371/journal.pone.0108763.

[10] H.R. Kataria and H.R. Patel, Radiation and chemical reaction effects on MHD Casson fluid flow past an oscillating vertical plate embedded in a porous medium, *Alexandria Engineering Journal* **55**(1) (2016), 583 – 595, DOI: 10.1016/j.aej.2016.01.019.

[11] G. Makanda, S. Shaw and P. Sibanda, Effects of radiation on MHD free convection of a Casson fluid from a horizontal circular cylinder with partial slip in a non-Darcy porous medium with viscous dissipation, *Boundary Value Problems* **2015** (2015), Article number: 75, DOI: 10.1186/s13661-015-0333-5.

[12] M.Y. Malik, M. Naseer, S. Nadeem and A. Rehman, The boundary layer flow of Casson nanofluid over a vertical exponentially stretching cylinder, *Applied Nanoscience* **4** (2014), 869 – 873, DOI: 10.1007/s13204-013-0267-0.

[13] M. Mustapha, T. Hayat, I. Pop and A. Aziz, Unsteady boundary layer flow of a Casson fluid due to an impulsively started moving flat plate, *Heat Transfer – Asian Research* **40**(6) (2011), 563 – 576, DOI: 10.1002/htj.20358.

[14] T. Salahuddin, M. Khan, T. Saeed, M. Ibrahim and Y.-M. Chue, Induced MHD impact on exponentially varying viscosity of Williamson fluid flow with variable conductivity and diffusivity, *Case Studies in Thermal Engineering* **25** (2021), 100895, DOI: 10.1016/j.csite.2021.100895.

[15] M. Tamoor, M. Waqas, M.I. Khan, A. Alsaedi and T. Hayat, Magnetohydrodynamic flow of Casson fluid over a stretching cylinder, *Results in Physics* **7** (2017), 498 – 502, DOI: 10.1016/j.rinp.2017.01.005.

[16] G.V. Vinogradov and A.Y. Malkin, *Rheology of Polymers*, Mir Publisher, Moscow (1979).

[17] W.P. Walwander, T.Y. Chen and D.F. Cala, An approximate casson fluid model for tube flow of blood, *Biorheology* **12**(2) (1975), 111 – 119, DOI: 10.3233/bir-1975-12202.